J. Chem. Sci. Vol. 124, No. 2, March 2012, pp. 385–393. © Indian Academy of Sciences.

Transition metal oxide loaded MCM catalysts for photocatalytic degradation of dyes

DIVYA JYOTHI[a], PARAG A DESHPANDE[b], B R VENUGOPAL[a], SRINIVASAN CHANDRASEKARAN[a] and GIRIDHAR MADRAS[b,*]

[a]Department of Organic Chemistry, Indian Institute of Science, Bangalore 560 012, India
[b]Department of Chemical Engineering, Indian Institute of Science, Bangalore 560 012, India
e-mail: giridhar@chemeng.iisc.ernet.in

MS received 22 March 2011; revised 26 May 2011; accepted 16 June 2011

Abstract. Transition metal oxide (TiO_2, Fe_2O_3, CoO) loaded MCM-41 and MCM-48 were synthesized by a two-step surfactant-based process. Nanoporous, high surface area compounds were obtained after calcination of the compounds. The catalysts were characterized by SEM, XRD, XPS, UV-vis and BET surface area analysis. The catalysts showed high activity for the photocatalytic degradation of both anionic and cationic dyes. The degradation of the dyes was described using Langmuir–Hinshelwood kinetics and the associated rate parameters were determined.

Keywords. Mesoporous materials; characterization; photocatalytic degradation; metal oxide doping.

1. Introduction

Among the various photocatalysts used for the treatment of industrial effluents, TiO_2 is the most widely used compound. Although several semiconductor materials have been tested for the photocatalytic degradation of dyes and other organic effluents, studies on TiO_2 have always remained the primary focus.[1] Several modifications of TiO_2 have also been carried out in order to enhance the quantum efficiency of the associated processes.[2,3]

One of the primary requirements for a good catalyst is to have a high surface area. In order to achieve this, there have been several formulations for the synthesis of TiO_2, which can restrict the crystallite size to nanometer dimensions. Nanosized TiO_2 has indeed proved to be a better catalyst showing higher photocatalytic activity[4,5] compared to that of the commercial TiO_2. In order to make efficient use of the available surface area of TiO_2, it is desirable to have a fine dispersion of TiO_2 on a high surface area material. This is similar to the dispersion of noble metals in a support for efficient use of the noble metal and one of the possible ways of achieving this is to disperse TiO_2 on high surface area zeolites.

Ordered mesoporous silica materials, owing to the three-dimensional networks, possess high surface area as well as high number of active sites for certain reactions. MCM compounds belong to this category of compounds and can be used as high surface area materials for dispersing TiO_2 nanoparticles. MCM-41 and MCM-48 are two such types of materials, differing in their structure. MCM-41 has a hexagonal structure while MCM-48 exhibits cubic structure. Both the materials have a large number of pores, interconnected to one another resulting in high surface area. Several investigators have reported the synthesis of highly ordered MCM-41 compounds using different techniques including sol–gel synthesis,[6] layer-by-layer method,[7] microemulsion method,[8] and cationic–anionic mixed gallery templates,[9] A detailed account of the various techniques employed for the synthesis of ordered mesoporous materials can be found elsewhere.[10]

The use of surfactants during the synthesis is desirable as it can aid to control the final microstructural properties of the material and it is possible to attain high degree of porosity, control over pore size distribution.[11] Therefore, in this study, we adopted one such route for the synthesis of MCM-41 and MCM-48. Due to the network structure, the synthesis of MCM-48 is more difficult as compared to the synthesis of MCM-41 and, therefore, there have been relatively more reports on the synthesis of MCM-41. However, the pore structure of MCM-48 makes it an interesting and important compound for catalytic applications. We have successfully synthesized high surface area MCM-41 and

*For correspondence

MCM-48 for their applications as support materials for photocatalysts.

Incorporation of TiO_2 in the mesoporous compounds has been reported by several investigators including the synthesis of nanocomposites as well as dispersion of TiO_2 in the material.[12–15] Several other compounds have also been incorporated in mesoporous materials for applications to both photocatalytic as well as non-photocatalytic reactions.[16–20] Apart from TiO_2, we have loaded Fe_2O_3 and CoO in MCM-41 and MCM-48 for photocatalytic reactions. Karunakaran *et al.*[21–25] have extensively studied semiconductor photocatalysis over a large number of oxide materials including Fe_2O_3. According to Karunakaran and Anilkumar,[25] Fe_2O_3 being a semiconductor, is a potential photocatalyst and on irradiation of UV radiation, the excitation of electron from valence to conduction band takes place resulting in the formation of electron-hole pairs, analogous to the electron-hole pair formation in TiO_2. The efficiency of the compounds may differ depending on the band gap and active surface groups. However, on the ground of similarity of the mechanism of reaction over TiO_2 and other oxides, it is desirable to explore the photocatalytic activity of Fe_2O_3 dispersed in MCM compounds. Zanjanchi *et al.*[26] have recently reported photocatalytic degradation of organics over sulphonated cobalt phthalocyanine – MCM-41 compound in which the organometallic group could be attached to MCM via the surface hydroxyl groups. The mechanism of reaction was proposed to be similar to the mechanism of oxide materials. There have also been reports on the photocatalytic activity of cobalt oxide-based compound.[27–29] Therefore, CoO was used in this study in the form of dispersion over MCM compounds and the compound indeed showed high activity for photocatalytic degradation of dyes. We present here a detailed synthesis of MCM-41 and MCM-48 via the surfactant assisted route, characterization of the compounds and modification of the compounds by impregnation of transition metal (Ti, Fe and Co) oxides for the photocatalytic degradation of dyes and kinetics of the degradation following the Langmuir–Hinshelwood mechanism. This is the first study reporting high photocatalytic activity of transition metal oxide-loaded MCM catalysts, synthesized via surfactant-assisted route, for the degradation of a range of anionic and cationic dyes.

The objectives of the study were manifold: (i) synthesis of high surface area ordered mesoporous MCM supports via the surfactant assisted route, (ii) obtaining a fine dispersion of transition metal oxide over the supports for potential photocatalysis, (iii) testing the photocatalytic activity of the composite catalysts for the degradation of dyes and comparing the activity with commercial photocatalysts and determining the kinetics of the photocatalytic degradation of dyes.

2. Materials and methods

2.1 *Synthesis of compounds*

2.1a *Synthesis of MCM-41*: Tetraethyl orthosilicate (TEOS) was used as the precursor for the synthesis of MCM-41 following a surfactant-assisted route using *n*-cetyltrimethylammonium bromide (CTAB) as the surfactant. A solution of CTAB in deionized water (2% by weight) was prepared. Ammonium hydroxide (NH_4OH, S.D. Fine Chem, India) and TEOS were subsequently added slowly with continuous stirring to obtain a gel of molar composition $TEOS:NH_4OH:CTAB:H_2O = 1:1.64:0.15:126$. Typically, 10 ml TEOS, 8 ml NH_4OH, 2.4 g of CTAB, and 120 g of deionized water were required to obtain the above composition. The gel was stirred for 12 h and the solid obtained was filtered, washed consecutively with water and ethanol, and calcined at 823 K for 5 h.

2.1b *Synthesis of MCM-48*: For the synthesis of MCM-48, 0.64 g sodium chloride (NaCl, S. D. Fine Chem, India) and 31.6 g of CTAB were dissolved in 83.4 g of deionized water. The solution was stirred until a clear solution was obtained. 2.68 g of sodium hydroxide (NaOH, S. D. Fine Chem, India) and 28.9 g of TEOS were dissolved in 68 g of deionized water, and stirred for 5 min. This solution was then added with the surfactant. A white gel precipitated during stirring for 15 min. The molar composition of the gel was CTAB: TEOS: NaCl: NaOH: $H_2O = 1:1.6:0.2:0.8:97$. The gel solution was transferred to a Teflon bottle and heated under static conditions at 373 K for 72 h. The precipitate was then filtered, washed several times with water, dried overnight at room temperature, and calcined at 823 K for 7 h under flowing air to remove the template.

2.1c *Synthesis of transition metal oxide-loaded MCM*: For the synthesis of transition metal oxide-loaded MCM, the mesoporous support material (MCM-41 or MCM-48) was heated at 110°C in an oven. Fe_2O_3 was loaded in the supports using iron (III) nitrate ($Fe(NO_3)_3{\cdot}9H_2O$ (S. D. Fine Chem, India) as the precursor.1.6 M $Fe(NO_3)_3{\cdot}9H_2O$ solution in water was added with MCM and the slurry was sonicated in a bath for 1 h. Excess water was drained out and the solids were dried at room temperature for 12 h. Water

was then removed by vacuum drying. The dried solids were washed with water and dried in an oven at 110°C for 4 h. The above procedure was repeated three times, and finally the solids were calcined at 450°C for 5 h to obtain iron oxide loaded MCM catalysts. Similarly, for obtaining TiO_2 and CoO loaded compounds, titanyl nitrate ($TiO(NO_3)_2$) and cobalt (II) nitrate (S. D. Fine Chem, India) were used, respectively. $TiO(NO_3)_2$ was obtained from nitration of titanium isopropoxide (Alfa Aesar, India). Calcination of TiO_2 and CoO loaded compounds was carried out at 350°C and 500°C, respectively.

2.2 *Characterization of compounds*

The compounds were characterized by scanning electron microscopy (SEM), low angle X-ray diffraction and powder diffraction (XRD), X-ray photoelectron spectroscopy (XPS), UV-vis spectroscopy, and BET surface area analyzer. SEM images were obtained from Quanta LV/ESEM machine; XRD patterns were recorded on Bruker machine (Bruker, Germany) equipped with CuKα source; XPS were recorded on Multilab ESCA instrument (Thermo, England); UV-vis spectra were recorded on Perkin Elmer Lambda 32 instrument and surface area analysis was carried out with NOVA-1000, Quantachrome apparatus with nitrogen adsorbent–desorption.

2.3 *Photocatalytic activity tests*

The photocatalytic degradation of dyes was carried out using a high pressure mercury lamp (Philips (125 W), India) which served as a source for UV radiation. The UV lamp radiated predominantly at 365 nm with an intensity of 26 W m^{-2}. The lamp was placed in a quartz tube which was equipped with a cooling jacket and cold water was continuously circulated to remove the heat generated by the lamp. Dye solution in water was placed in a dish beneath the UV lamp, over a magnetic stirrer. 50 ml of 50 ppm dye solution was added with 50 mg of the catalyst and the solution was stirred using the magnetic stirrer. The solution was stirred in the absence of UV light for 2 h to observe the adsorption of the dye over the catalyst surface and allow the adsorption equilibrium to be attained. This ensures that the decrease in concentration of the dyes observed is due to photocatalytic degradation and not due to adsorption. The solution was then irradiated with UV light and the samples were taken for analysis at regular intervals of time. The samples were then centrifuged and analysed using UV-visible spectrophotometer (UV 1700, Shimadzu, Japan). The variation of the concentration of the dye with time was determined from the calibration plot, obtained from the absorbance of the dye solutions of different concentrations. Further details on the experimental procedure can be found elsewhere.[5]

3. Results and discussion

3.1 *Structural analysis*

SEM images were recorded for studying the microstructure and morphology of the catalysts. Figure 1 shows the SEM images of the different MCM-based compounds. Spherical particles can be observed in figures 1(a,b) for both MCM-41 and MCM-48 catalysts. Well-separated particles can be seen for both the catalysts. It can be seen that the particles were not in fused state and large void spaces were present in the compounds. However, the voidage, as can be seen from the SEM imaged differed for different compounds. Whereas well-separated spherical particles can be observed for pure and Ti-based compounds (figures 1a–d), fusion of the particles can be observed for Co and Fe-based compounds (figures 1e,f). This was very prominent for MCM-48-Fe (figure 1f) The diameters of the particles were in the range of 200–500 nm. The average particle diameter was smaller for MCM-41, however, a large difference between the particle sizes of MCM-41 and MCM-48 was not observed. Similarly, for the case of MCM-41-Ti and MCM-48-Ti, well-separated spherical particles were observed (figures 1(c,d)). No significant difference in the size of the particles was observed on impregnation of TiO_2 in the support MCM materials. However, with impregnation of Fe_2O_3 and CoO, small changes in the morphology of the particles were observed. Flake-like particles were observed for MCM-48-Co (figure 1(e)). Further, the particles were also observed to have higher degree of polydispersity compared to that for MCM-41, MCM-48 or Ti loaded-MCM. The size of the particles for both MCM-48-Co and MCM-48-Fe was found to be larger. For the case of MCM-48-Fe, larger agglomerates having smaller particles can be observed. The higher particle size can be a result of higher calcinations temperature during the synthesis of the compounds.

The amount of metal oxide in the sample was small. The X-ray dispersive spectra (EDS) for all the compounds were recorded. EDS of all the compounds are provided in figure S1 (supplementary information). The

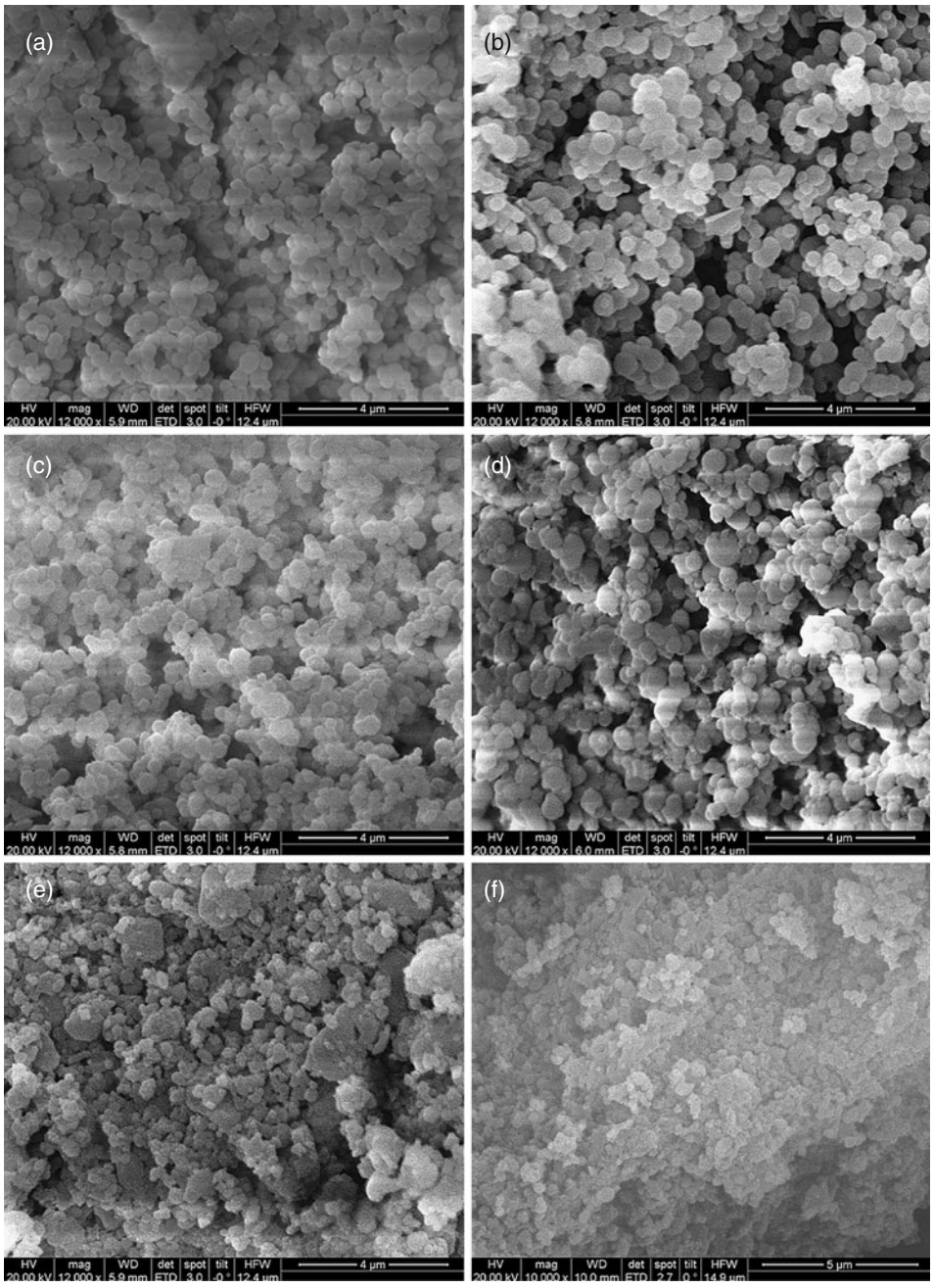

Figure 1. SEM images of the various catalysts. (**a**) MCM-41, (**b**) MCM-48, (**c**) MCM-41-Ti, (**d**) MCM-48-Ti, (**e**) MCM-41-Co, (**f**) MCM-48-Fe.

presence of Ti, Co and Fe in the compounds was confirmed from the spectra.

The crystal structure of all the compounds was confirmed by XRD patterns. The small angle XRD patterns of all the compounds are provided in figure S2 (supplementary information). MCM-41 was found to crystallize in hexagonal structure whereas MCM-48 was found to crystallize in cubic structure. Powder XRD of TiO_2-loaded MCM was also recorded. Because the amount of TiO_2 in the sample was only 3.8 wt% in MCM-41-Ti and 4.5 wt% in MCM-48-Ti (as confirmed by EDS), no intense peaks corresponding to TiO_2 was observed in the XRD patterns. However, the formation of TiO_2 (and other oxides) was confirmed by XPS studies.

The XPS of Ti2p in MCM-41-Ti and MCM-48-Ti is shown in figure 2(a). The binding energy of 459 eV corresponds to Ti in +4 oxidation state. This confirmed that Ti was present as TiO_2 in the compounds. Similarly, the spectra of Fe2p and Co2p are shown in figures 2(b) and (c), respectively. Fe can be observed to be in +3 state

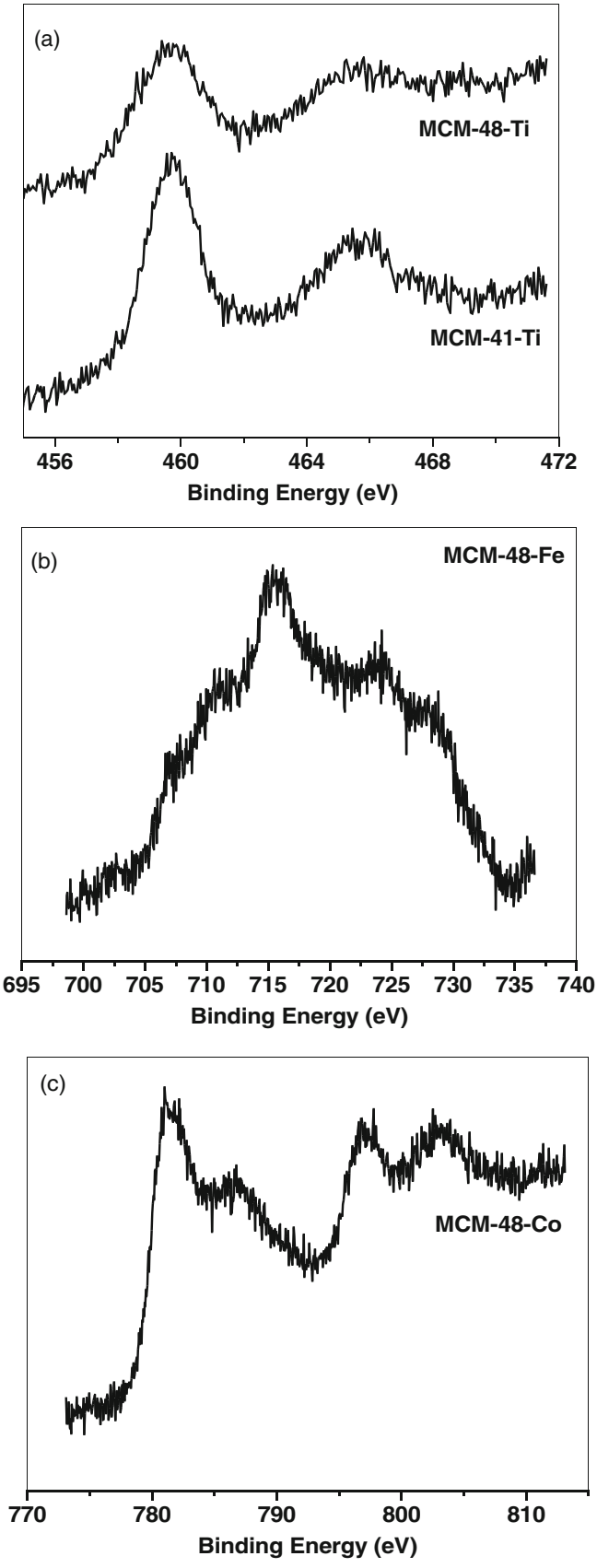

Figure 2. X-ray photoelectron spectra of (**a**) Ti2p, (**b**) Fe2p, (**c**) Co2p.

and Co can be observed to be in +2 state, corresponding to Fe_2O_3 and CoO, respectively. This confirms the formation of oxides and the impregnation of metals in oxide form.

N_2 adsorption–desorption curves for MCM-41 and MCM-48 are shown in figure 3. The surface areas obtained were 870 m^2/g for MCM-41 and 1000 m^2/g for MCM-48. The pore size for MCM-41 and MCM-48 was found to be 2.6 nm and 4.6 nm, respectively. Therefore, the compounds synthesized were nanoporous, high surface area compounds.

The UV-vis spectra of all the compounds are shown in figure 4. The spectra were used for the determination of the band gap using the absorption edge. For wavelength edge of λ nm, the band gap is given as $E_g = 1240/\lambda$. MCM-41, MCM-48, and MCM-48-Ti showed similar absorbance characteristics and the band gap for the compounds was found to be 3.36 eV. For MCM-41-Ti and MCM-48-Fe, band gaps were similar with a value of 2.96 eV. MCM-48-Co, however, showed two distinct values of absorbance and two absorbance edges at 420 nm and 696 nm were observed. Therefore, the compound showed two band gaps of 2.96 eV and 1.78 eV corresponding to 420 nm and 696 nm, respectively. The presence of multiple band gaps is known, especially in case of doped materials.[30] Arktla *et al.*[31] have reported the synthesis of MCM-41 and no significant UV absorption was observed. In the current study, we have not only found the bare MCM-41 to be photocatalytically active but a decrease in the band gap was also observed on introduction of TiO_2 nanoparticles. A decrease in band gap on the use of ordered mesoporous materials has also been observed by Cojocaru *et al.*[32]

3.2 *Photocatalytic activity*

Indigo carmine (IC) was chosen as a model dye for testing the photocatalytic activity of MCM and transition metal oxide-loaded MCM catalysts. The variation of normalized IC concentration with time over the different catalysts is shown in figure 5. In a control experiment in which no catalyst was added (photolysis), nearly 16% degradation was observed in 1 h. On addition of catalysts, an increase in conversions was observed, as can be seen from figure 5. More than 50% conversion was observed in 1 h when the reaction was carried out in presence of MCM-41. The initial rate of degradation was observed to increase further when TiO_2-loaded MCM-41 (MCM-41-Ti) was used. Nearly 80% conversion was observed with MCM-41-Ti in 1 h compared to 50% conversion with MCM-41. It should

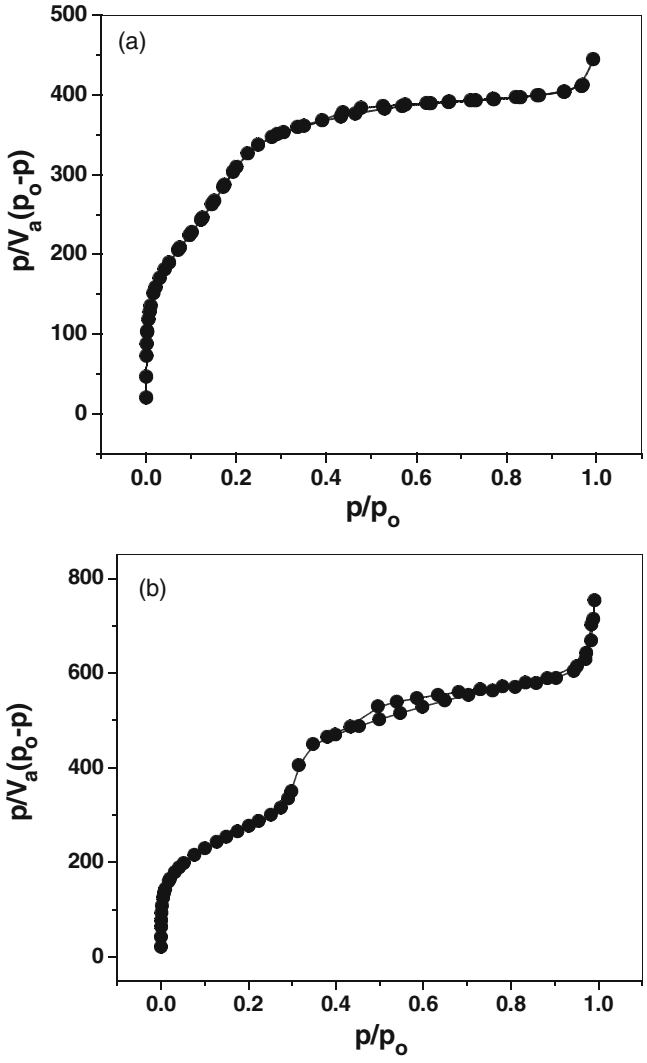

Figure 3. N_2 adsorption–desorption profile for (**a**) MCM-41, (**b**) MCM-48.

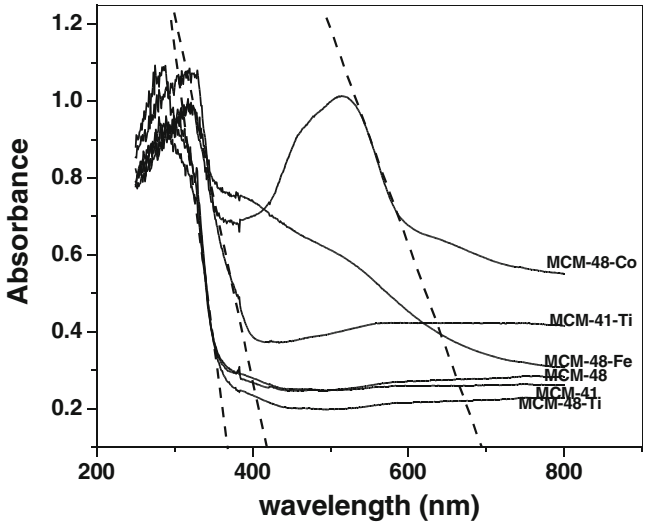

Figure 4. UV-vis spectra of the various catalysts.

be noted that whereas MCM-based compounds have been used as adsorbents for both liquids and gases, no appreciable adsorption of the dyes was observed in the present study. All the results shown in the figure correspond to the decrease in the concentration of the dye on irradiation of the dye solution in the presence of the catalyst. Whereas no appreciable decrease in the concentration of the dyes was observed on stirring the dye solution with the catalyst for 2 h, a large decrease in the dye concentration was observed on irradiation. This clearly indicated the photocatalytic activity of the catalyst and not the adsorption of the dye over the high surface area compounds. The adsorption of the dyes is highly pH and site-specific and therefore, it is possible that in spite of having a large surface area, appreciable adsorption did not take place for the dyes used in this study.

MCM-48 showed lesser activity for the photocatalytic degradation of the dye compared to MCM-41. Only 20% degradation was possible within 1 h. However, a large enhancement in the photocatalytic activity of the catalyst was observed on impregnation with Fe_2O_3 (MCM-48-Fe), TiO_2 (MCM-48-Ti) and CoO (MCM-48-Co). Nearly 30% conversion was obtained with MCM-48-Fe and 40% conversion was obtained over MCM-48-Ti. The rate of degradation over MCM-48-Co was found to be the highest with almost complete degradation achieved within 30 min of reaction. Degradation was also carried out with commercial Degussa P-25 TiO_2 catalyst (DP25). It is to be noted that only 3–4 wt% of TiO_2 was present in the samples compared to 100% TiO_2 in DP25. It can be observed from figure

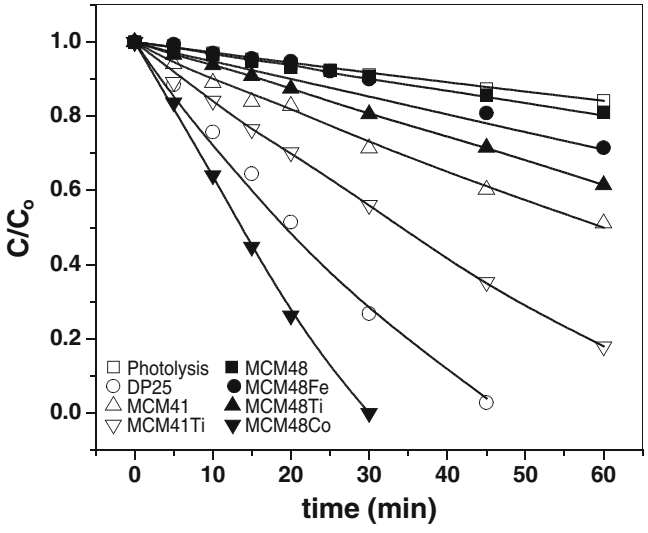

Figure 5. Variation of normalized concentration of IC with time over the different catalysts.

5 that almost complete conversion was possible within 45 min over DP25. However, MCM-48-Co showed better activity than DP25. The high activity of the compound can be a result of a fine dispersion of the oxide over a large surface area. Whereas the surface area of DP-25 is limited to only 50 m^2/g, the surface areas of the compounds reported in this study exceed 1000 m^2/g. A fine dispersion of the particles in a very high surface area support result in high activity of the compound. Whereas further investigation for the synergistic effects due to the presence of active species in both MCM and oxides are required, the presence of synergism cannot be completely rejected.

SiO_2 has a band gap of 8.9 eV[33] rendering it useless for photocatalytic applications. However, it has to be noted that although MCM compounds have Si–O–Si framework in their structure, they exhibit different optical characteristics. Photoluminescence measurements on MCM-41 and MCM-48 by Shen and Cheng[34] have revealed factors responsible for photoluminesence and the strucural features can be attributed for the same. Non-bridging oxygen hold centers present in the compounds make the electron transfers and excitation possible in MCM compounds unlike SiO_2.

A possible reason for difference in the behaviour of the two supports can be the difference in the pore sizes. The surface areas obtained were 870 m^2/g for MCM-41 and 1000 m^2/g for MCM-48. The pore size for MCM-41 and MCM-48 was found to be 2.6 nm and 4.6 nm, respectively. Upon loading TiO_2, the surface areas decreased to 780 and 890 m^2/g for MCM-41 and MCM-48, respectively. Nevertheless, the surface area of the materials discussed in this study is much higher than commercial DP-25 TiO_2 (50 m^2/g), which is used for UV-assisted photocatalysis. The average pore diameters also reduce to 2.3 and 4.1 nm for TiO_2-loaded MCM-41 and MCM-48, respectively. The reduction of the surface area and the average pore diameter has been reported in other studies.[35,36] The size of the dye is 15.66 × 5.52 × 4.08 $Å^3$. Due to the large size of 1.5 nm of the dye, it may pose diffusional limitations. The active sites in the compounds are present in the porous structure and diffusion of the reactants is required for the reaction to take place. The impregnation of the oxides might result in the blockage of the pores thereby reducing the activity of the catalyst.

Having established high activity of MCM-48-Co for the photocatalytic degradation of IC, a series of anionic and cationic dyes were tested for photocatalytic degradation. The anionic dyes tested were orange G (OG), remazol brilliant blue R (RBBR), alizarin cyanine green (ACG); the cationic dyes tested were methylene blue (MB), acriflavin (AF), and malachite green (MG). The variation of normalized concentration (initial concentration = 50 ppm) with time is shown in figure 6. It can be seen that the compound showed activity for the degradation of all the dyes. The degradation of anionic dyes was higher compared to the degradation of cationic dyes with more than 90% degradation of ACG and RBBR observed in 1 h. MG also showed high degradation with nearly 85% degradation observed in 1 h. AF and MB showed nearly the same extent of degradation and 40–45% degradation was observed.

The kinetics of the degradation reaction is conventionally described by the Langmuir–Hinshelwood kinetics, which takes into account the adsorption of the dye over the surface of the catalyst, surface reaction and desorption of the products. The rate of reaction following Langmuir–Hinshelwood kinetics can be given as

$$r = \frac{kK_eC}{1 + K_eC}, \tag{1}$$

where r is the rate of degradation of dye, k is the rate constant for the degradation of the dye, K_e is the adsorption equilibrium constant and C is the concentration of the dye in the solution. We have previously tested the kinetics of the degradation of dyes over the various catalysts by proposing the elementary steps and Langmuir–Hinshelwood kinetics was found to describe the kinetics of the reaction.[5,37–40] In this study, we test the kinetics of the degradation following the Langmuir–Hinshelwood kinetics and determine the corresponding rate parameters. The continuous lines in figures 5 and 6 show the variation of normalized dye concentration

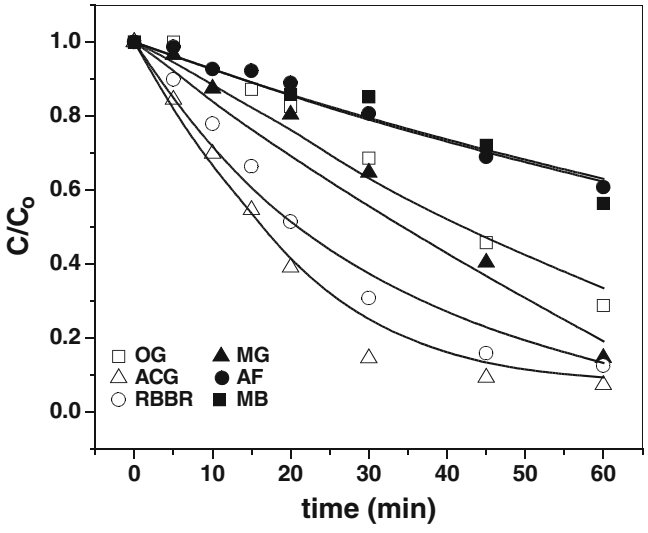

Figure 6. Variation of normalized concentration of different anionic and cationic dyes over MCM-48-Co.

Table 1. Rate parameters describing the kinetics of degradation of IC over different catalysts following Langmuir–Hinshelwood kinetics.

Catalyst	k_1 ($\times 10^3$) (min^{-1})	k_2 ($\times 10^3$) (ppm^{-1})
Photolysis	3.0	–
DP25	37.8	1.3
MCM-41	12.3	0.66
MCM-41-Ti	23.2	26.3
MCM-48	3.8	17.1
MCM-48-Fe	6.1	0.56
MCM-48-Ti	9.1	0.51
MCM-48-Co	59.6	1.4

with time correlated by Langmuir-Hinshelwood kinetics, except for the case of photolysis where first order decay was assumed. It can be observed from figures 5 and 6 that the variation of concentration for all the cases could be satisfactorily described by Langmuir–Hinshelwood kinetics. The associated rate parameters for reaction were determined by simultaneously solving the above differential equation with a time step of 5×10^{-4} min and minimizing the least square errors using Berkeley Medonna software (version 8.3.18). The values of adsorption and rate parameters are tabulated in tables 1 and 2 where $kK_e = k_1$ and $K_e = k_2$. It can be clearly seen from tables 1 and 2 that the rate of reaction was the highest over MCM-48-Co and the least over MCM-48 for the degradation of IC. For the degradation of other dyes over MCM-48-Co, the rate of degradation was found to follow the order IC > ACG > RBBR > MG > OG > MB ≈ AF.

We have previously studied in detail the degradation of dyes over TiO_2 catalyst and studied the effect of functional group on the reactivity of the dyes.[40] The trend observed in this study is in agreement with our previous studies. The ease for formation of intermediates and breakage of different bonds depend upon the functional groups present in the dye. The hydroxylation reaction, which is one of the most important reactions in the degradation of the dyes, is affected by the presence of the various groups present in the dye. The presence of atoms like N and S, and their combination result in different bonds with different strengths and hence, different ease of breakage of the bond. The presence of the position of the substituent groups also affects the various primary and secondary hydroxylation processes and hence, the activity of the catalyst is strongly dependent upon the identity of the dye.

Table 2. Rate parameters describing the kinetics of degradation of different dyes over MCM-48-Co following Langmuir–Hinshelwood kinetics.

Dye	k_1 ($\times 10^3$) (min^{-1})	k_2 ($\times 10^3$) (ppm^{-1})
OG	15.3	0.70
RBBR	33.7	0.76
ACG	46.1	0.78
MB	7.9	0.22
AF	7.7	0.17
MG	19.0	1.00
IC	59.6	1.4

For the case of S atom, the ease of degradation of the dye depends on the identity of the oxygenated S species formed during the reaction and their position of attachment in the dye or the intermediate. When the $-SO_3^-$ group is attached to the benzene ring, it shows higher reactivity than if it was attached to a naphthalene ring. Thus a high degradation of IC, which contains two benzene rings with attached $-SO_3^-$, is observed. Similarly, ACG, which has one benzene ring with attached $-SO_3^-$, shows a higher degradation rate compared to the azo dye (OG), where $-SO_3^-$ is attached to the naphthalene ring. The degradation of acridine dyes requires a much complex reaction pathway involving de-methylation followed by a sequential breakage of benzene rings and ring opening and thus the degradation rates of AF are lower than other dyes. A detailed discussion on the effect of functional groups on the photocatalytic degradation of dyes can be found in our previous work.[40]

The high activity of MCM-48-Co can be explained on the basis of band gap. CoO was loaded in MCM-48, which had a very high surface area. The compound not only showed a lesser band gap but also multiple band gaps, owing to which high activity of the compound was observed. Even when the amount of CoO in the compound was very small, the compound showed the activity which was higher than that of the commercial DP25 catalyst because of both high surface area as well as lower value of the band gap. Similarly, the activity of MCM-48, MCM-48-Fe and MCM-48-Ti followed the order of activity as MCM-48 < MCM-48-Fe < MCM-48-Ti owing to their respective values of band gap.

4. Conclusions

Surfactant-assisted synthesis of MCM-41 and MCM-48 resulted in the formation of high surface area compounds. Nano-sized TiO_2, Fe_2O_3 and CoO were loaded in the supports and the compounds were tested for the photocatalytic degradation of indigo carmine dye. The

compounds showed high activity for the degradation of IC in the presence of UV radiation. The rates of reaction were found to be higher over MCM-41 compared to MCM-48. However, on impregnation of oxides, MCM-48 was found to be a better support and very high rates of degradation of IC were observed. MCM-48-Co was found to be the best catalyst among the tested materials and degradation rate increased an order of magnitude on CoO impregnation in MCM-48. The rates of degradation over MCM-48-Co were found to be higher than the commercial DP25 catalyst. The reaction coefficients were determined for the degradation of dyes and the reasons for the high photocatalytic activity was discussed.

Supplementary information

Figures S1 and S2 are given as supplementary information (see www.ias.ac.in/chemsci).

Acknowledgements

The funding from the Indo-French Centre for the Promotion of Advanced Research and the Department of Science and Technology (DST), Govt. of India, are gratefully acknowledged.

References

1. Hoffmann M R, Martin S T, Choi W and Bahnemann D W 1995 *Chem. Rev.* **95** 69
2. Chen X and Mao S S 2007 *Chem. Rev.* **107** 2891
3. Thompson T L and Yates, Jr. J T 2006 *Chem. Rev.* **106** 4428
4. Nagaveni K, Hegde M S, Ravishankar N, Subbanna G N and Madras G 2004 *Langmuir* **20** 2900
5. Sivalingam G, Nagaveni K, Hegde M S and Madras G 2003 *Appl. Catal. B: Environ.* **45** 23
6. Liu X, Sun H and Yang Y 2008 *J. Colloid Interf. Sci.* **319** 377
7. Sadasivan S and Sukhorukov G B 2006 *J. Colloid Interf. Sci.* **304** 437
8. Weidenkaff A 2004 *Adv. Eng. Mater.* **6** 709
9. Mao H, Li B, Li X, Yue L, Liu Z and Ma W 2010 *Ind. Eng. Chem. Res.* **49** 583
10. Valdes-Solis T and Fuertes A B 2006 *Mater. Res. Bull.* **41** 2187
11. Goltner C G and Antonietti M 1997 *Adv. Mater.* **9** 431
12. Zanjanchi M A, Golmodeh H and Arvind M 2009 *J. Hazard. Mater.* **169** 233
13. Yang H, Deng Y and Du C 2009 *Coll. Surf. A.* **339** 111
14. Mihai G D, Meynen V, Beyers E, Mertens M, Bilba N, Cool P and Vansant E F 2009 *J. Porous. Mater.* **16** 109
15. Sun B, Reddy E P and Panagiotis P G 2005 *Appl. Catal. B: Environ.* **57** 139
16. Signoretto M, Ghedini E, Trevisan V, Bianchi C L, Ongaro M and Cruciani G 2010 *Appl. Catal. B: Environ.* **95** 130
17. Parida K M and Rath D 2009 *J. Colloid Interf. Sci.* **340** 209
18. Liu H, Lu G, Guo Y, Wang Y and Guo Y 2010 *J. Colloid Interf. Sci.* **346** 486
19. Zheng Y, Li Z, Zheng Y, Shen X and Lin L 2006 *Mater. Lett.* **60** 3221
20. Hua D, Chen S, Yuan G and Wang Y 2010 *J. Porous. Mater.* doi:10.1007/s10934-010-9434-9
21. Karunakaran C and Senthivelan S 2006 *Electrochem. Commun.* **8** 95
22. Karunakaran C and Dhanalakshmi R 2009 *Radiation Phys. Chem.* **78** 8–12
23. Karunakaran C, Dhanalakshmi R and Karuthapandian S 2005 *J. Photochem. Photobiol. A: Chem.* **170** 233–238
24. Karunakaran C and Anilkumar P 2007 *J. Mol. Catal. A: Chem.* **265** 153
25. Karunakaran C and Anilkumar P 2008 *Solar Energy Mater. Solar Cell.* **92** 490
26. Zanjachi M A, Ebrahimian A and Arvand M 2010 *J. Hazard. Mater.* **175** 992
27. Bai J 2009 *Mater. Lett.* **63** 1485
28. Yang Q, Choi H, Al-Abed S R, Dionysiou D D 2009 *Appl. Catal. B: Environ.* **88** 462
29. Chiang K, Amal R and Tran T 2002 *Adv. Environ. Res.* **6** 471
30. Khan S U M, Al-Shahry M and Ingler Jr. W B 2002 *Science* **297** 2243
31. Artkla S, Kim W, Choi W and Wittayakun J 2009 *Appl. Catal. B: Environ.* **91** 157
32. Cojocaru B, Neatu S, Parvulescu V I, Dumbuya K, Steinruck H-P, Gottfried J M, Aprile C, Garcia H and Scaiano J C 2009 *Phys. Chem. Chem. Phys.* **11** 5569
33. Laughlin R B 1980 *Phys. Rev. B* **22** 3021
34. Shen J L and Cheng C F 2003 *Curr. Opinion Solid State Mater. Sci.* **7** 427
35. Strunk J, Vining W C and Bell A T 2010 *J. Phys. Chem. C* **114** 16937
36. Reddy E, Davydov L and Smirniotis P G 2002 *J. Phys. Chem. B* **106** 3394
37. Priya M H and Madras G 2006 *J. Photochem. Photobio.* **178** 1
38. Aarthi T and Madras G 2007 *Ind. Eng. Chem. Res.* **46** 7
39. Aarthi T, Narahari P and Madras G 2007 *J. Hazard. Mater.* **149** 725
40. Vinu R, Akki S U and Madras G 2010 *J. Hazard. Mater.* **176** 765